acceptance of this article, the publisher or recipient acknowledges the U.S. Government's right to retain a non - exclusive, royalty - free license in and to any copyright covering the article.

NUCLEUS-NUCLEUS POTENTIALS

Conf-830340--1

CONF-830340--1

DE83 009799

G. R. SATCHLER

Oak Ridge National Laboratory, Physics Division
Oak Ridge, Tennessee 37830

Abstract: The significance of a nucleus-nucleus potential is discussed. Information about such potentials obtained from scattering experiments is reviewed, including recent examples of so-called 'rainbow' scattering that probe the potential at smaller distances. The evidence for interactions involving the nuclear spins is summarized, and their possible origin in couplings to non-elastic channels. Various models of the potentials are discussed.

1. Introduction

2. Meaning of a nucleus-nucleus potential

   2.1 Feshbach projection theory

   2.2 Resonating-group/generator-coordinate theories

   2.3 Other interaction potentials

3. What do we learn from experiments?

   3.1 Low energies and the strong-absorption radius

   3.2 The nuclear stratosphere

   3.3 Potentials at smaller distances and incomplete absorption

      3.3.1 Refractive effects

      3.3.2 'Rainbow' scattering

      3.3.3 'Anomalous large-angle scattering' and model independent potentials

   3.4 Potentials from fusion barriers

   3.5 Spin dependence

4. Some potential models

   4.1 Interaction energy functions

   4.2 Folding model

   4.3 Surface interactions

Talk to be presented at the Conference on Heavy-Ion Physics
Catania, Italy, March 21-26, 1983

MASTER

DISTRIBUTION OF THIS DOCUMENT IS UNLIMITED

NUCLEUS-NUCLEUS POTENTIALS

G. R. SATCHLER

Oak Ridge National Laboratory, Physics Division
Oak Ridge, Tennessee 37830

Abstract: The significance of a nucleus-nucleus potential is discussed. Information about such potentials obtained from scattering experiments is reviewed, including recent examples of so-called 'rainbow' scattering that probe the potential at smaller distances. The evidence for interactions involving the nuclear spins is summarized, and their possible origin in couplings to non-elastic channels. Various models of the potentials are discussed.

1. Introduction

Usually the first step in a description of the collision of two nuclei is the introduction of a simple one-body potential that describes some gross features of the scattering. This provides a basis upon which a more detailed description may be built. The DWBA treatment of non-elastic transitions is a well-known example[1]. Another is that almost all models of the fusion of two nuclei introduce an interaction potential which, together with the Coulomb field, provides a potential barrier[2]. In these various ways, elastic scattering is treated as a doorway through which the system must go before other processes are manifest, whether they be direct reactions, deep-inelastic scattering or complete fusion. Nucleus-nucleus potentials play important roles in other phenomena also, such as quasi-molecular resonances.

Naturally, we try to incorporate into such potentials as much of the known physics as is possible or practical. This includes choosing the potentials to reflect the overall sizes of the interacting nuclei and making them complex so that they accommodate the loss of flux ('absorption') into other, non-elastic, channels. Conversely, we hope to obtain more information about the physics by studying the properties of phenomenological potentials required to fit the measurements, such as on elastic scattering and fusion reactions.

Although only a sub-field of nuclear physics, the subject of potentials in general, and elastic scattering in particular, is already too broad to be reviewed in detail here. (For a somewhat wider discussion, and other references to the literature, see ref. 1, for example.) Rather, a few topics of particular interest have been selected and (bearing in mind the admonitions of the conference organizers) the approach is more didactic than just a review of the latest results. In contrast to most discussions of light-ion scattering, in heavy-ion physics we frequently encounter the use of classical terms like 'trajectories' and 'rainbows'. These are often useful aids to thought, even though they are never appropriate in a literal sense because of diffractive effects and the presence of absorption.

2. Meaning of a nucleus-nucleus potential

2.1 FESHBACH PROJECTION THEORY

Unfortunately there is not a unique prescription for the nucleus-nucleus potential. For example, in theories of the type developed by Feshbach[1,3] an effective interaction appears which is defined as that object which, when used in a one-body Schrödinger equation

$$[-(\hbar^2/2\mu)\nabla^2 + \mathcal{V}]\chi_{00}(\underset{\sim}{r}) = E\,\chi_{00}(\underset{\sim}{r}) \qquad (1)$$

(where μ is the reduced mass of the colliding pair and E is their relative kinetic energy), reproduces the wavefunction for relative motion $\chi_{00}(\underset{\sim}{r})$ of that part of the total wavefunction in which the two colliding nuclei both remain in their ground states. (Even that statement requires qualification when anti-symmetrization is taken into account properly. The identification of the separation of the centers of mass of the two nuclei is not unique when they overlap because of the indistinguishability of the nucleons.) This part of the wavefunction may be very small in the region of space where the two nuclei interact strongly.

Although a substantial contribution to the real part of $\mathcal{V}$ is expected to be the folded potential U_F to be discussed below,

$$\mathcal{V} = U_F + \Delta U, \tag{2}$$

the remainder ΔU, sometimes referred to as the dynamic polarization potential, is very complicated (complex, non-local, energy-, and angular momentum-dependent). It contains the effects of the couplings to non-elastic channels, including the loss of flux (absorption) into these channels, as well as any consequences of anti-symmetrization that are not already included in U_F. If we ignore anti-symmetrization between the two nuclei, the effective interaction may be written in the familiar form

$$\mathcal{V} = (\psi_0,\phi_0|V|\psi_0\phi_0) + (\psi_0\phi_0|VQ\,\frac{1}{E-H_{QQ}+i\epsilon}\,QV|\psi_0\phi_0), \tag{3}$$

where ψ_0,ϕ_0 are the internal wavefunctions for the two nuclei in their ground states, while Q projects on to all the excited states. We may then identify the first term of (3) as the folded potential U_F and the remaining term as ΔU. In principle, V is a sum of bare nucleon-nucleon interactions between the two nuclei; however, because of the strong, short-ranged repulsion, some kind of Brueckner transformation is frequently assumed so that V itself becomes an effective (or G-matrix) interaction which already includes some 'polarization' corrections, primarily those associated with the short-ranged correlation between the interacting nucleons; thus there may be an element of double-counting when this interaction is used in eq. (3). This effective interaction may also be complex, density-dependent and energy-dependent.

In principle, some averaging over the microstructure is also needed before a reasonable formal identification of as an optical model interaction can be made. In phenomenological approaches, it is this which is approximated in eq. (1) by a local, complex optical model potential $U_{OM}(r)$, with the optical model equation

$$[-(\hbar^2/2\mu)\nabla^2 + U_{OM}(r)]\chi_{OM}(\underset{\sim}{r}) = E\,\chi_{OM}(\underset{\sim}{r}). \tag{4}$$

One consequence is that the corresponding optical model wavefunction $\chi_{OM}(\underset{\sim}{r})$ is no longer identical to the exact $\chi_{00}(\underset{\sim}{r})$ of eq. (1) (if only because of the corrections for non-locality). Even if U_{OM} is adjusted to give the observed elastic scattering, so that χ_{OM} and χ_{00} are the same asymptotically, they will differ in the interaction region where the separation distance r is small and the two nuclei overlap.

Equation (3) is merely a formal rearrangement of the original problem and is scarcely any easier to solve. However, such formal manipulations frequently exhibit more clearly the structure that a solution must have and which should be incorporated, as far as possible, into any model U_{OM}.

2.2 RESONATING-GROUP/GENERATOR-COORDINATE THEORIES

The aim of the Feshbach theory is to define a potential operator to be used in the usual form (1) of one-body Schrödinger equations, whose solution describes the motion of the two nuclei while they remain in their ground states (with due regard for the ambiguity of that condition when they overlap). The RGM/GCM types

of theories can also be manipulated to yield Schrödinger equations[4,5]. These theories take antisymmetrization into account fully in a straightforward way.

If a one-channel trial wavefunction is used, a one-body Schrödinger equation like (1) results, and the associated (non-local) potential is real (unless a complex effective interaction V was used). When trial functions involving more than one channel are considered, the result is a set of coupled-channel equations. These may be reduced to one-channel equations like (1) and (3) by the same type of channel elimination procedures, with the same attendant complications. Unfortunately, computational difficulties have restricted most applications of these approaches to models with one or very few channels, whereas typical heavy-ion collisions involve very large numbers of open channels. One-channel RGM calculations have provided insights into the importance of corrections[4,6] to the folding models discussed below due to the exchange of nucleons between the two nuclei because of antisymmetrization, though still leaving unresolved the problem as to whether these results are seriously affected by the presence of strong absorption (i.e. the coupling to many non-elastic channels).

2.3 OTHER INTERACTION POTENTIALS

It is not always true that other ways of calculating a nucleus-nucleus interaction energy result in something that can be directly interpreted as a potential to be used in the one-body Schrödinger equation (1) or (4) (see particularly the discussion in ref. 5). In microscopic approaches a total energy curve is calculated as a function of the distance separating the two nuclei (as before, care must be taken over the definition of this distance when the two nuclei overlap). Often this energy curve is interpreted as a potential and used in eq. (4) to calculate the elastic scattering. Strictly this is incorrect. These calculations may use the energy-density approach, the Thomas-Fermi or Hartree-Fock approximations, the liquid-drop model, the proximity theorem, etc., but they all attempt to follow explicitly to a greater or lesser degree the readjustments that the two nuclei must make as they begin to interact and overlap; distortion of the nuclear shapes, reaction to the Pauli principle, effects of the saturating nature of nuclear forces, etc. Such an interaction energy function does not determine just the ground-state component $\chi_{00}(\underset{\sim}{r})$ of the wavefunction, but is related to the motion of a wavepacket which includes a wide range of excited states of the separated systems. Such a wavepacket may be appropriate for describing the evolution of a process like fusion[2], but the ground-state component must be projected out asymptotically before it can describe elastic scattering. Thus the calculated potential is not to be identified with the operator of eqs. (1) and (3), even though the consequences for elastic scattering of the same physical excitation processes are manifested in the polarization potential term ΔU in eq. (2). Even when the calculation is performed (as it frequently is) in the adiabatic approximation, so that the systems do return finally to the elastic channel, corrections to the kinetic energy term of eq. (1) are required. For example, the mass parameter in the interaction region is not the reduced mass of two point masses, but itself depends upon r. It is possible that the model equations may be recast into the form (4) by transforming the corrections into an effective potential (see ref. 7 for a recent discussion of this and ref. 8 for an early example). We also note in passing that the adiabatic approximation results in a real potential; there is no absorption, no loss of flux to other channels. Thus the potential has to be supplemented by a phenomenological imaginary potential in scattering calculations. There is a certain inconsistency in this procedure, especially when the absorption is strong.

Thus we see that there is more than one way of formulating the nucleus-nucleus potential problem and the corresponding scattering solutions $\chi(\underset{\sim}{r})$ will differ (and require different interpretations) in the overlap region even if they give the same elastic scattering, so that $\chi(\underset{\sim}{r}) \to \chi_{00}(\underset{\sim}{r})$ at large r. In some ways the Feshbach formalism of eq. (3) is the most transparent, yet also this expression is deceptively simple. It is most convenient to use when the effects of just a few non-elastic channels are to be studied explicitly. The energy-surface approaches provide vehicles for including, perhaps in intuitively more

obvious ways, various bulk physical effects. It is instructive to contrast this situation with the scattering of nucleons from nuclei. In that case the optical potential is much better understood in terms like eq. (3), and is closely related to the Hartree-Fock potential for bound states. Other light ions, being composite nuclei, share most of the problems just discussed for heavy ions.

3. What do we learn from experiments?

Here we consider what properties we need for a phenomenological, local, optical model potential U(r), used in eq. (4), in order to interpret various experimental data on heavy-ion collisions. In a general sense, heavy-ion collisions are associated with strong absorption; i.e. intimate contact leads to non-elastic events and absorption from the elastic channel. Consequently, the scattering is dominated by conditions at the surface, and it is difficult (in many cases, impossible) to learn about U(r) at small values of r. (Here, 'surface' means the region in r where the nuclear forces begin to act strongly.) Against this background, an important question is: how deeply can various measurements probe the nucleus-nucleus potential?

3.1 LOW ENERGIES AND THE STRONG-ABSORPTION RADIUS

The majority of heavy-ion elastic scattering data have been obtained at relatively low bombarding energies ($\lesssim$ 10 MeV per nucleon) which often are not very far above the Coulomb barrier. Their angular distributions usually show the characteristic Fresnel or Fraunhofer diffraction patterns[9]. It is well known[1] that under these circumstances the scattering is "only sensitive to the potential in the vicinity of the strong absorption radius, R_{SA}". Clearly, it is incompatible with quantum mechanics to say that we can determine the potential at a single point; what is implied is that there is a particularly sensitive region centered near R_{SA} and a fermi or so in extent[11]. Given good data, together with the constraint that there is strong absorption at smaller radii, we can then obtain quite accurate values for the real and imaginary parts of the potential in this region as well as some information about their slopes.

This strong absorption radius can be defined in various (but similar) ways; for example, as the distance of closest approach of a classical Rutherford trajectory with the same angular momentum as that for which the optical model transmission coefficient is one-half, or (in the case of Fresnel-like scattering) one corresponding to the scattering angle for which the observed cross section has fallen to one-fourth of the Rutherford value, etc. Typically the values of R_{SA} are given approximately by

$$R_{SA} \approx 1.5(A_1^{1/3} + A_2^{1/3})\ \text{fm}, \quad \text{or} \quad R_{SA} \approx 1.1(A_1^{1/3} + A_2^{1/3}) + 2.5\ \text{fm}. \qquad (5)$$

Physically, the variation with A is better represented[10] by the latter, which corresponds roughly to a constant separation between the half-central-density points of the two nuclei. The noteworthy feature is that the values of R_{SA} are quite large; the nuclei are barely tickling each other (see fig. 1 for an example). However, the onset of the strong but short-ranged nuclear forces is so sudden that approaches somewhat inside R_{SA} lead to removal from the elastic channel. Thus it is the character of the potential in this region that determines precisely how the transition from no absorption to essentially complete absorption takes place. The values of the attractive real potential near R_{SA} are typically[12] one to a few MeV and are reproduced quite well by theoretically constructed potentials[13-16]. On general grounds, one expects the potential to be well represented by an exponential in this region, with a strength proportional to the mean radius of curvature of the surfaces of the two nuclei, or

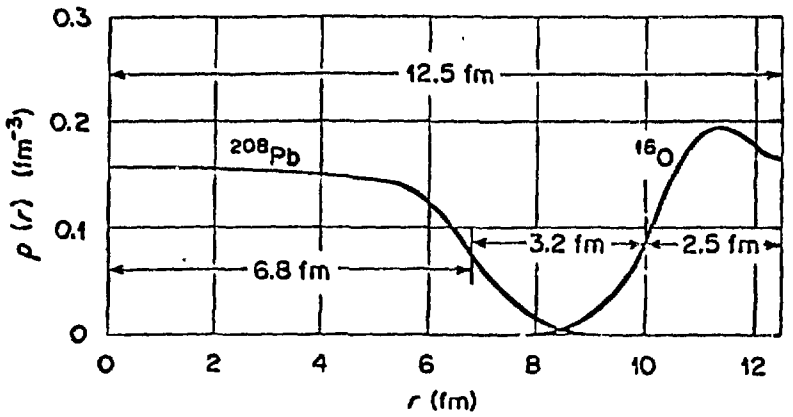

Fig. 1 Showing the density overlap for $^{16}O + ^{208}Pb$ ions at the strong absorption radius for scattering at ~ 100-200 MeV.

$$\mathrm{Re}U(r) \approx -S_o \frac{R_1R_2}{R_1+R_2} \exp\left[-\frac{r-R_1-R_2}{\alpha}\right], \qquad r \approx R_{SA}. \tag{6}$$

Empirically, $\alpha \sim 0.65$ fm and the strength constant $S_0 \sim 60$ MeV. There is little or no evidence for any dependence on bombarding energy.

3.2 THE NUCLEAR STRATOSPHERE

The situation just related has been known for a number of years. Of more interest, perhaps, is learning about the potential in other regions. At one extreme have been recent attempts[17] to "probe the nuclear stratosphere", namely measurements of deviations from Rutherford scattering at energies significantly below the Coulomb barrier so the nuclei only interact at large distances, several fermi beyond R_{SA}. Various corrections (atomic screening, vacuum polarization, virtual excitation of the giant dipole resonance, relativistic effects, etc.) must be made very carefully before nuclear potentials can be extracted.

3.3 POTENTIALS AT SMALLER DISTANCES AND INCOMPLETE ABSORPTION

In the other direction, there are a number of scatterings which appear to probe the potential at distances smaller than R_{SA}. By necessity, these must involve incomplete absorption, at least in the surface region. We consider three categories.

3.3.1 Refractive effects

Much insight is provided by formally decomposing the scattering amplitude into 'near-side' and 'far-side' components[1,9,18], $f(\theta) = f_N(\theta) + f_F(\theta)$. These have a simple interpretation when $\lambda\!\!\!^{-} \ll R_{SA}$, as for heavy ions, which is illustrated in fig. 2 for scattering from a strongly absorbing sphere. The amplitude is predominantly Rutherford, $f_C(\theta)$, for small scattering angles, but this term is eliminated by absorption in the shadow region, for angles greater than θ_g which corresponds to a grazing collision. In addition, there are amplitudes corresponding to the wavelets diffracted from the far- and near-side edges. These have profiles peaked at $\pm\,\theta_g$ and with exponential decays into the classically forbidden regions, as indicated in fig. 3. Thus the far-side contribution corresponds to diffractive scattering to 'negative' angles. When the Coulomb repulsion is sufficiently strong, the far and near grazing trajectories diverge so much that only the near-side amplitude is significant; this is the case for Fresnel-like angular distributions[9]. The divergence decreases at energies further above the Coulomb barrier, and we begin to see oscillations for $\theta > \theta_g$ due to interference between the two terms. In the limit this becomes the Fraunhofer diffraction pattern[9].

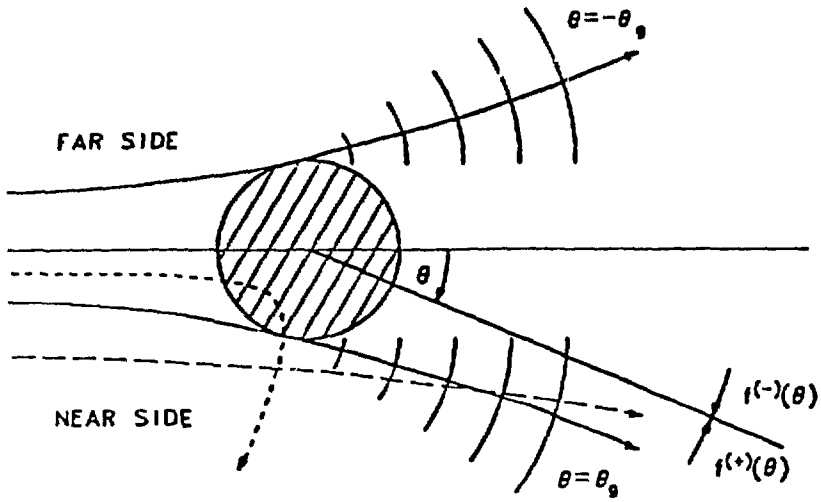

Fig. 2 Illustrating classical trajectories and waves diffracted from the near and far sides of a strongly absorbing region. The solid curves represent classical grazing trajectories which suffer diffraction at the edge of the 'black' sphere. The long-dashed curve is a Rutherford trajectory for a large-impact parameter, which experiences little diffraction. The short-dashed curve is a Rutherford trajectory for a small impact parameter, which is strongly absorbed.

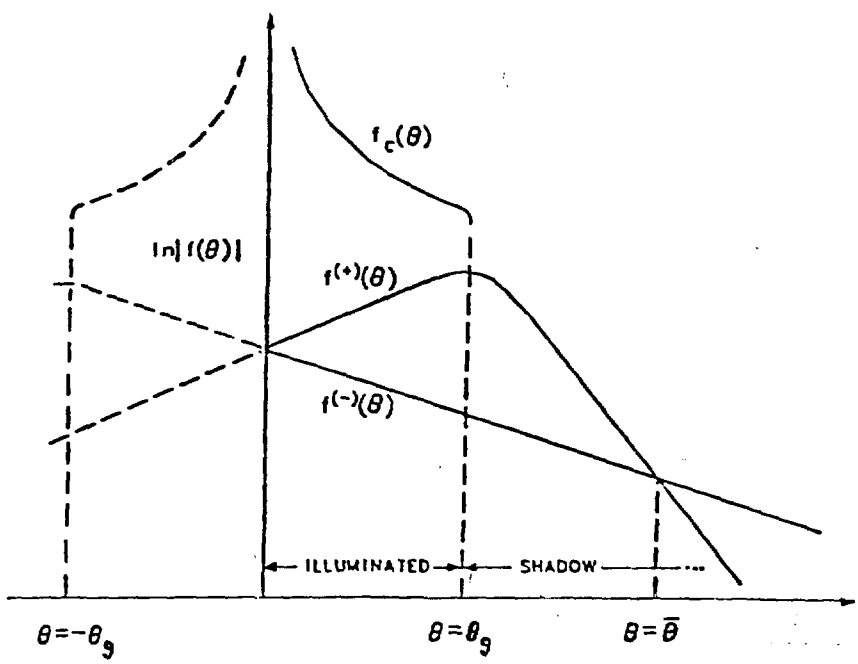

Fig. 3 Angular distributions of the near-side and far-side amplitudes, where (+) denotes near side and (-) denotes far side.

When we include a short-ranged nuclear attraction at the surface of the sphere, this enhances the waves diffracted from the far side and (for $\theta > \theta_g$) reduces those from the near side. The amplitude profiles become asymmetric about $\theta = \theta_g$ (fig. 3). These properties can be exhibited formally in a simple model of the scattering amplitude[1,9,18,19] which gives for $\theta > \theta_g$

$$f_N(\theta) \propto (\sin\theta)^{-1/2}\, e^{-i\Lambda\theta}\, e^{-(\pi+\alpha)\Delta(\theta-\theta_g)}, \tag{7a}$$

$$f_F(\theta) \propto (\sin\theta)^{-1/2}\, e^{i\Lambda\theta}\, e^{-(\pi-\alpha)\Delta(\theta+\theta_g)}. \tag{7b}$$

Here Λ is the angular momentum for the grazing collision and Δ, which determines the angular width of the fan of diffracted waves from each edge, is related to the surface diffuseness. The (positive) parameter α is a measure of the effects due to refraction at the surface by the attractive nuclear potential; its character can be seen from its approximate relation to the potential U(r) in the surface region[18],

$$\tan\alpha \approx \mathrm{Re}U(r)/\mathrm{Im}U(r). \tag{8}$$

This shows how refractive effects depend upon the balance between the strengths of absorption and attraction in the surface.

The phase factors $\exp(\pm i\Lambda\theta)$ in (7) mean that interference between f_N and f_F gives oscillations with a period in θ of π/Λ. However, in the absence of refraction ($\alpha = 0$), f_F is smaller than f_N by the factor $\exp(-2\pi\Delta\theta_g)$. This changes dramatically when $\alpha \neq 0$, for then the two terms have different slopes (fig. 3) and, indeed, the far-side term is the larger one for $\theta > \bar{\theta} = (\pi/\alpha)\theta_g$. The resulting angular distribution is very characteristic (fig. 4). When observed, it allows

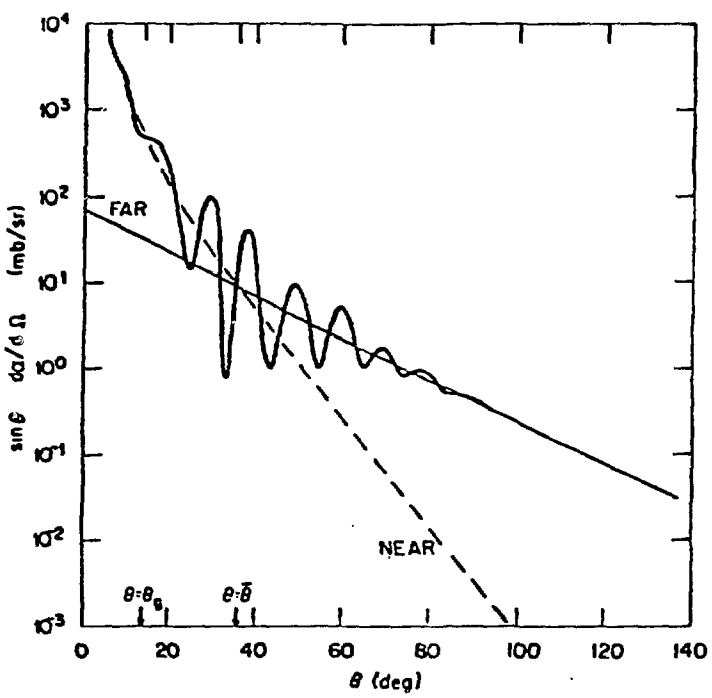

Fig. 4 Far-side/near-side decomposition in the presence of strong absorption plus refraction at the surface.

one to place constraints on the strength of the real potential in the surface, at distances somewhat inside R_{SA}.

This effect has been seen for ^{6}Li + ^{28}Si at 135 MeV[20] and 154 MeV[21]. As fig. 5 shows, a shallow Woods-Saxon potential can fit the oscillations for $\theta \lesssim 25°$ but a potential that is deeper for $r < R_{SA}$ is required to reproduce the tail of the far-side amplitude seen for $\theta \gtrsim 40°$. Indeed it has been shown[21] that fits to these data are sensitive to the real potential for $r \approx 4$ fm (ReU $\approx$ -60 MeV) to 8 fm (ReU $\approx$ -1 MeV), whereas $R_{SA} \approx 7$ fm. Measurements on ^{12}C and ^{16}O + ^{28}Si at energies near 200 MeV did not show this characteristic angular distribution (fig. 5) and are only sensitive to the real potential at larger radii[22] because of the stronger surface absorption in these cases. (It is curious that ^{28}Si should be more 'transparent' to the loosely bound ^{6}Li than to the tighter clusters ^{12}C and ^{16}O!) This led to the suggestion[20] that there was a qualitative change in the scattering characteristics (from "light ion" to "heavy ion") for projectile masses between 6 and 12. However, since then a similar pattern has been seen for ^{12}C + ^{12}C at 300 MeV[23] (fig. 6) and some indications of it at 289 MeV and 1016 MeV[24,25], as well as further evidence for ^{6}Li on ^{12}C and ^{40}Ca at 156 MeV[26].

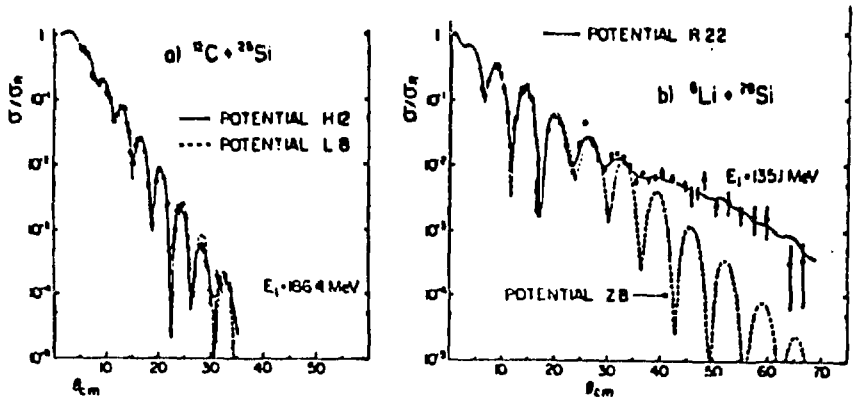

Fig. 5 Heavy-ion scattering with (right) and without (left) marked refractive effects. The Z8 potential for ^{6}Li is a shallow one similar to the H12 for ^{12}C, while R22 and L8 are more attractive for $r < R_{SA}$.

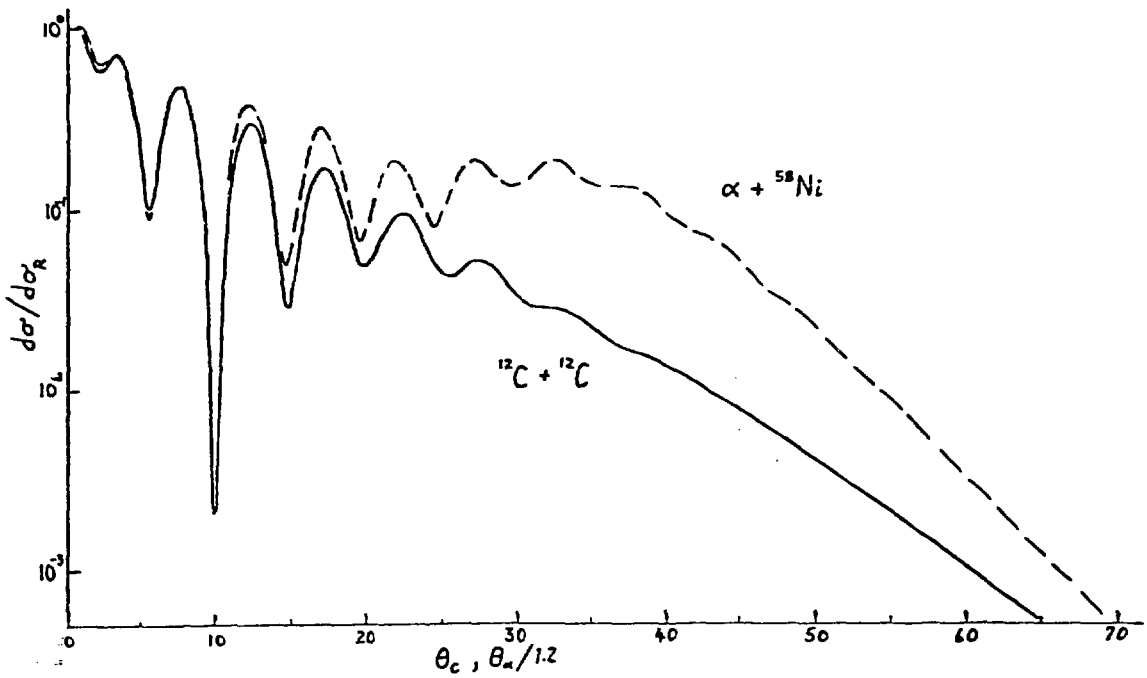

Fig. 6 Comparison of optical model fits to $^{12}C + ^{12}C$ at 300 MeV and $\alpha + ^{58}Ni$ at 139 MeV. (The curves follow the data closely over the whole range shown.)

If the 156-MeV $^{6}Li+^{12}C$ data are fitted using a local optical potential, the real potential values are determined[26] quite accurately over a range of radii from $r \approx 2.5$ fm (ReU ≈ -80 MeV) to $r \approx 7$ fm (ReU ≈ -1 MeV). In the case of $^{12}C + ^{12}C$ at 300 MeV, we can determine the potential from $r \approx 4$ fm (ReU ≈ -60 MeV) to $r \approx 7$ fm (ReU ≈ -1 MeV), whatever form (Woods-Saxon, folded, proximity, etc.) is assumed for it. Scattering at 1 GeV extends this region of sensitivity to somewhat smaller radii by about 1 fm[24,25]; this possibility is indicated by the optical model absorption profiles shown in fig. 7. These distances correspond to a substantial overlap of the densities of the two ^{12}C nuclei (fig. 7) and thus

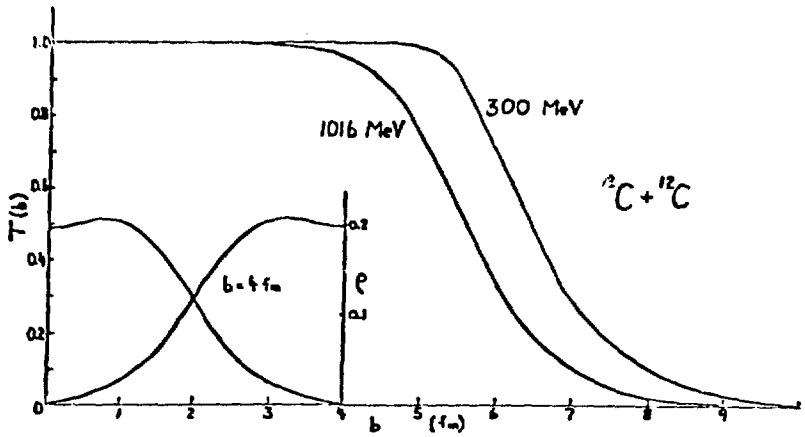

Fig. 7 Transmission profile for $^{12}C + ^{12}C$ at 300 MeV and 1016 MeV. $T_L = 1 - |S_L|^2$ plotted vs. impact parameter $b = L/k$. Inset: density profiles when $r = 4$ fm.

provide severe tests of our ideas about the meaning of such potentials (see discussion of Sec. 2). These various $^{12}C+^{12}C$ data sets cover a wide range of energies, and provide one of the first unequivocal pieces of evidence for an energy dependence in the optical potential for heavy ions. At 1 GeV, the potential in the surface has the same shape as at 300 MeV but is nearly a factor of two weaker[24].

3.3.2 'Rainbow' scattering

The appearance in the cross section of an exponential-like fall-off, such as seen in fig. 4, is often cited as evidence for nuclear rainbow scattering. This usage of the word seems to be inappropriate, so we should now briefly discuss rainbows.

As the absorption is weakened, refraction becomes more important until in the limit we have scattering by a real potential. Then, when the wavelength is sufficiently short, the language of classical particle scattering can be used (with caution!). The scattering properties are conveniently embodied in the deflection function (fig. 8), whose quantal generalization is frequently defined as

$$\Theta(L) = 2 \text{ Re } (d\delta_L/dL),$$

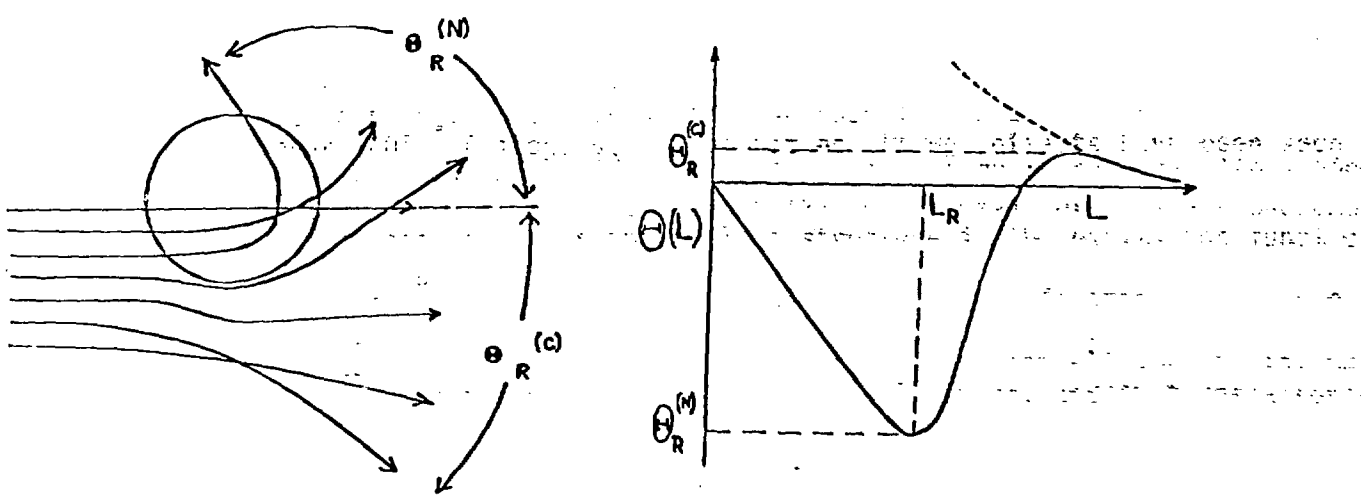

Fig. 8 Left: classical trajectories leading to Coulomb (C) and nuclear (N) rainbows. Right: Deflection function.

where δ_L is the Lth partial wave phase shift (nuclear plus Coulomb). A rainbow occurs whenever $\Theta(L)$ has an extremum $\Theta(L) = \Theta_R$, corresponding to an enhancement in the cross section at that angle. (In the classical limit, $d\sigma/d\theta \propto |d\Theta/dL|^{-1}$.) The 'Coulomb' rainbow at large L corresponds to crossing the Coulomb barrier. The inner one is called a 'nuclear' rainbow because it depends upon the nuclear potential at smaller distances. Because such a rainbow corresponds to negative-angle scattering, it appears as a modification of the far-side component of the scattering amplitude. A residuum of this classical feature survives a surprising amount of absorption and can be observed in the angular distributions for alpha scattering at energies $\gtrsim$ 100 MeV[27]. Figure 6 provides an example for $\alpha + {}^{58}Ni$ at 139 MeV; the 'hump' in the angular distribution around 40° is the signature of the rainbow, followed by the smooth fall-off on the dark side. Since θ_R becomes more negative as the nuclear potential becomes more attractive, the observation of this rainbow feature helps one to determine the real potential.

Such a distinctive hump is not observed in the ${}^{6}Li$ scattering of fig. 5, nor the ${}^{12}C+{}^{12}C$ case of fig. 6. Indeed, examination of the scattering matrix elements for ${}^{12}C + {}^{12}C$ at 300 MeV shows that the partial waves in the vicinity of the rainbow are strongly absorbed, $|S_L| \approx 0.002$ for $L \approx L_R$. In fact, we may put $|S_L| = 0$ for all partial waves with L up to several units greater than L_R without noticeably affecting the fit to the data. This is in contrast to the $\alpha + {}^{58}Ni$ case, where $|S_L| \approx 0.03$ is an order of magnitude larger for $L \approx L_R$ and the cross section is sensitive to S_L for the small L-values. (Note that, in one sense, this still is "strong" absorption, since $T_L = 1 - |S_L|^2 \approx 0.999$. Quite small transmissions are sufficient to produce observable effects.) In addition, a decomposition of the ${}^{12}C+{}^{12}C$ amplitude into far and near components reveals[28] a pattern like that shown in fig. 4, with no rainbow feature in the far-side term. Only if the absorption is artificially reduced does a true rainbow emerge. Consequently, there seems to be little justification for using the name 'rainbow' for the ${}^{12}C+{}^{12}C$ scattering, even though it is refractive enough to allow the characteristic far-side amplitude to be observed and thus to determine the real potential in some region of the inner surface. The situation may be different at the higher energy of 1 GeV, where the absorption is significantly weaker for the partial waves associated with the classical rainbow, $|S_L| \approx 0.1$ for $L \approx L_R$.

3.3.3 'Anomalous large-angle scattering' and model-independent potentials

In addition to the 'high-energy' data just discussed, there are a number of cases of heavy-ion scattering at lower energies which, if described in terms of potential scattering, imply incomplete absorption at least within the inner surface and, to that extent, say something about the potential at smaller distances. The prototype 'anomalous large-angle scattering' (ALAS) was observed for $\alpha + {}^{40}Ca$ at energies of ~ 20-50 MeV, called anomalous because, after a rapid decrease at forward angles, the cross section rose to values larger than the Rutherford one near 180°. Analogous, though not as strong, effects have been seen for some heavy-ion systems: ${}^{16}O + {}^{28}Si$ (energies of 30 to 60 MeV), ${}^{16}O + {}^{40}Ca$ (54 MeV), ${}^{6}Li + {}^{40}Ca$ (30 MeV), ${}^{6}Li + {}^{28}Si$ (27 and 34 MeV), etc. These phenomena are also associated with a resonance-like structure in the excitation functions for large scattering angles.

It has been shown that these data can be understood in terms of potential scattering provided the real potential is sufficiently deep to sustain a pocket in the total nuclear + Coulomb + centrifugal 'potential' for partial waves with impact parameters smaller than the grazing wave, and that the absorption is sufficiently 'weak' to allow non-zero $|S_L|$ values (~ a few %) for these waves. Whether or not one decides finally that this is a useful way to describe these phenomena, it is of interest that scattering by simple potentials can exhibit this kind of behavior.

The observation of oscillatory structure in an angular distribution suggests the interference between two sub-amplitudes (c.f. Sec. 3.3.1). In this case, the WKB approximation has been used[18,29] to decompose the scattering amplitude into 'barrier' (B) and 'internal' (I) parts,

$$S_L = S_L^{(B)} + S_L^{(I)}, \tag{9}$$

corresponding to reflection from the outer barrier, and from the centrifugal barrier at the inner face of the pocket in the total 'potential' (see left side of fig. 9). If the absorption in the pocket is strong, the inner reflected wave is

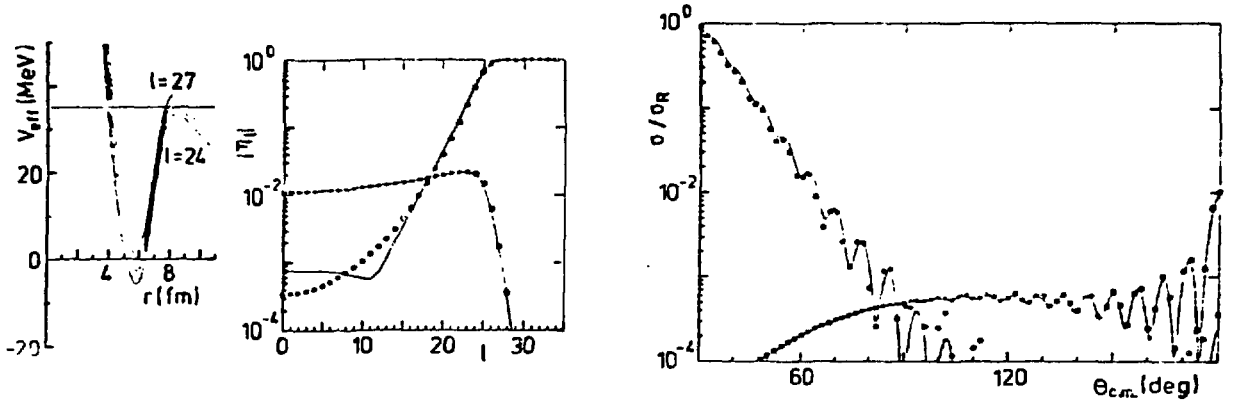

Fig. 9 'Barrier' and 'inner' decomposition[30] for $^{16}O + ^{28}Si$ at 55 MeV. Left: nuclear + Coulomb + centrifugal potential for grazing waves. Center: decomposition of partial wave scattering elements $|S_L|$. Right: cross sections due to B and I waves separately (no interference shown). The B amplitude by itself shows evidence for far-side/near-side interference.

completely damped, $S_L^{(I)} \to 0$. Consequently, observation of the effects due to this contribution implies incomplete absorption inside the pocket region and the possibility of gaining information on the real potential there. A number of decompositions following eq. (9) have been made for heavy-ion systems[1,11].

Early optical potential analyses of such data were made using conventional Woods-Saxon forms, later generalized to other shapes such as Woods-Saxon-squared. More recently, so-called model-independent techniques have been used. These may add to a conventional potential, a limited Fourier-Bessel series whose coefficients are adjusted to fit the data. Another technique is to specify the values of the potential at a number of radial points and use a spline interpolation between them. These methods provide a controlled way of generalizing from simple analytic forms. They also provide error bands that reveal the regions of sensitivity for a given fit, although it has to be remembered that the uncertainties at different radii are correlated. Frequently the scattering is found to be less sensitive to the precise shape of the imaginary potential, so that conventional 'volume' and 'surface' Woods-Saxon forms are used, the added flexibility being reserved for the real potential.

Many such analyses have been made for alpha scattering[31], which, for medium weight targets, often determine the potential down to within one or two fermis of the center. Applications[32-39] to the scattering of heavier ions have given more ambiguous results, presumably because the absorption is usually stronger. For example, for $^{16}O + ^{40}Ca$ at 50 MeV, one may obtain[36] two or more potentials which give equally acceptable fits to the data, depending upon the starting points used. These potentials differ considerably even in the surface region, and result in quite different scattering matrix elements[36], implying a 'phase-shift ambiguity' also for this particular data set. One lesson to be learned from these and other studies is that the successful use of these techniques requires very precise and extensive data. Another is that fully unconstrained potentials have limited

usefulness; for systematic results, it is important to input some prejudice. An example of this is a study[37] of $^{16}O + ^{28}Si$ at seven energies from 30 to 55 MeV, using data that extend out to 180°. Use of a completely model-independent real potential revealed substantial (discrete) ambiguities and potentials with pronounced structures that did not vary in a systematic way. Consequently, a constraint was introduced by using as a fixed reference potential one that was a very deep (673 MeV at r = 0) folded one, supplemented by a spline-interpolated correction ΔU confined to the surface region $r > 5$ fm, together with a Woods-Saxon and its derivative for the imaginary part.

The fits to the data were as good as those obtained with the unconstrained potentials; they are shown in fig. 10. The corresponding potentials are shown in fig. 11. The real significance of these results lies in their systematic behavior, despite the fluctuations from energy to energy. (Note that the data themselves involve incomplete averaging over fine structure ~ 200 KeV that an optical model is not expected to reproduce.) The real, spline, correction ΔU is similar in character at all energies and qualitatively like that obtained[40] from eq. (3) due to coupling to inelastic channels. Although the ΔU almost certainly depends upon the choice of reference potential, its qualitative features are probably more general. Sensitivity tests indicated that ΔU is determined down to about $r \approx 6$ fm at 31.6 MeV. The imaginary potentials also show fluctuations in their detailed shapes, but show one striking feature that their radial extent shrinks as the energy falls; i.e. they exhibit more surface transparency at the lower energies.

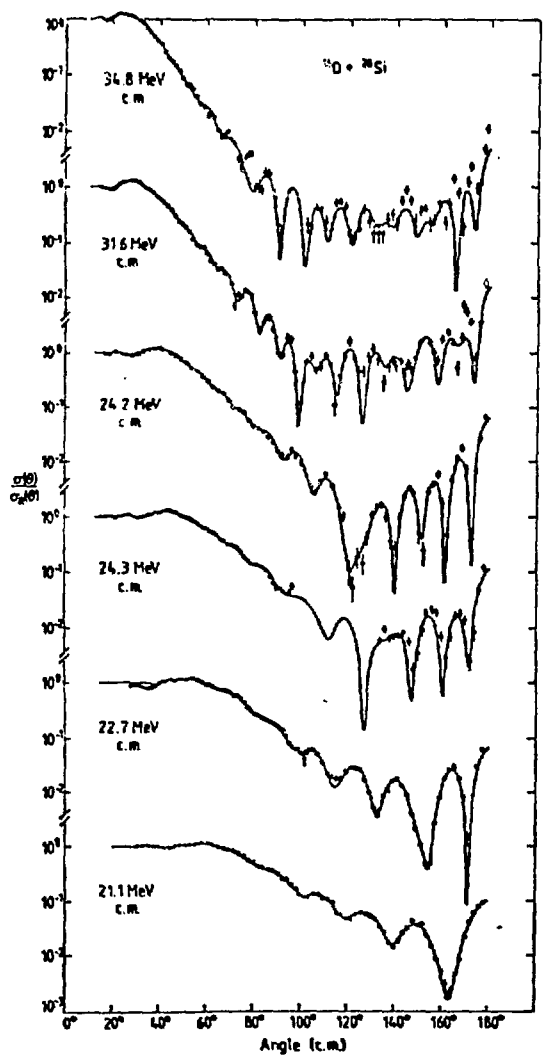

Fig. 10 Model-independent potential fits[37] to $^{16}O + ^{28}Si$.

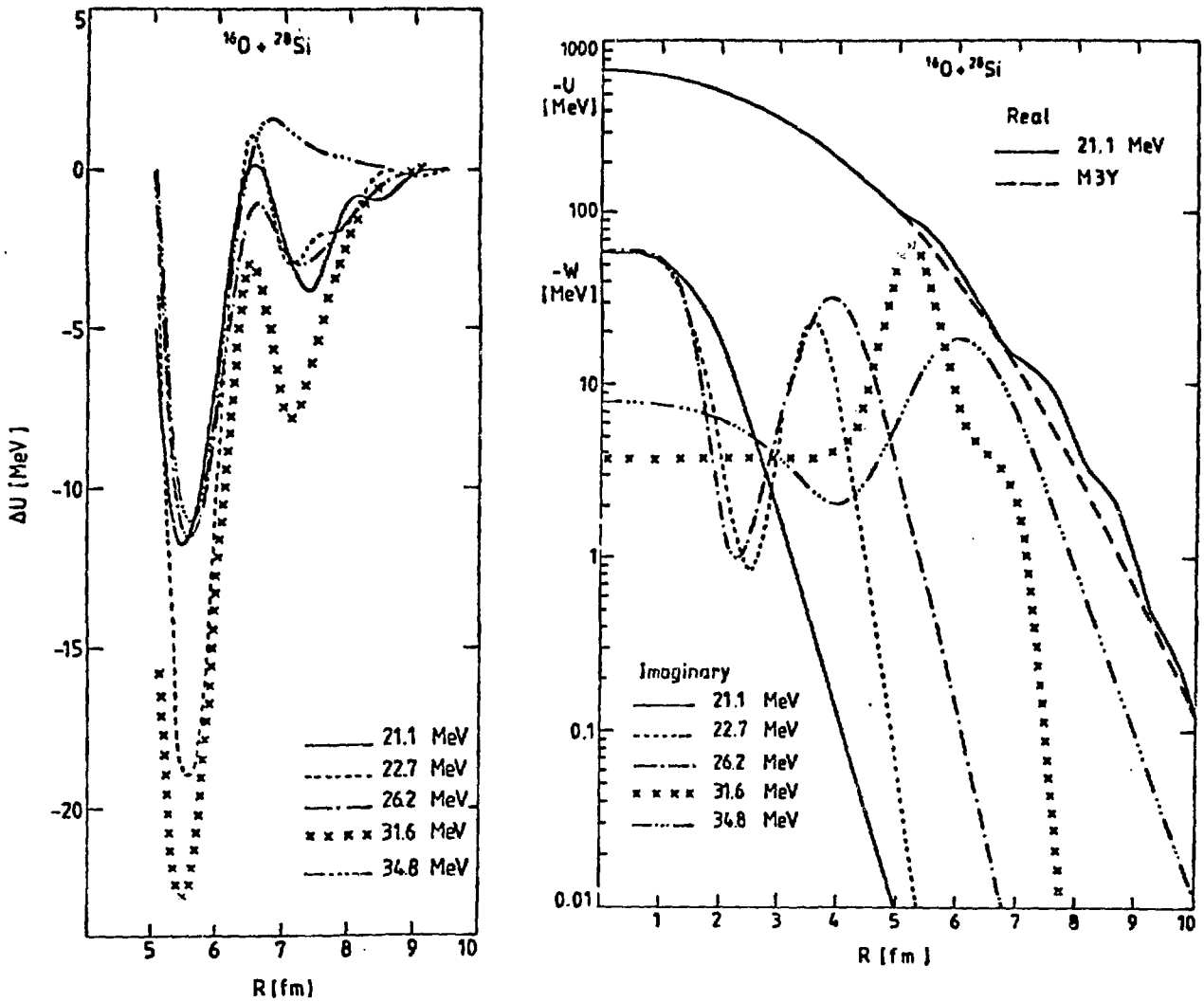

Fig. 11 Potentials corresponding to fits[37] in fig. 10. Left: model-independent real correction. Right: imaginary potentials W(r), and the real folded (M3Y) reference potential. Also shown in the corrected real potential at 21.1 MeV.

This behavior can be reproduced by making the radius parameters depend linearly on energy,

$$r_W(E_{CM}) \approx r_W(E_{CM} = 26.2)[1 + \delta(E)], \qquad \delta(E) \approx 0.055(E_{CM} - 26.2). \qquad (10)$$

This prescription also reproduces the main features of the excitation function at 180°.

Another interesting ALAS case concerns $^6Li + ^{28}Si$ at 27 and 34 MeV[39] measured out to 175°. Woods-Saxon-squared or folded shapes for the real potential, with central depths ~ 200 MeV, gave the best fits. A model-independent Fourier-Bessel analysis indicated that there was no discrete ambiguity in this case and that the real potential was essentially determined from 2 or 3 fm out to about 9 fm. This indicates another example of incomplete absorption in the interior.

3.4 POTENTIALS FROM FUSION BARRIERS

At energies close to their Coulomb barrier, the fusion of two nuclei is frequently assumed[2] to be a barrier penetration process. Thus measurements give a measure of the attractive nuclear potential at that position. This extends our knowledge of the nucleus-nucleus interaction somewhat inside the strong absorption radius for low-energy elastic scattering, although (see Sec. 2) it is not obvious that the same 'potential' is involved. In any case, the potential values extracted are generally in good agreement with theoretical expectations[13,14,41].

At higher energies, a critical radius $r = R_{cr}$ is introduced[42] and, in the potential barrier model, the fusion cross section is determined by this radius and the value of the potential there. Since R_{cr} is appreciably smaller than the barrier radius, this provides information on the potential inside the barrier. Figure 12 summarizes[43] the values of the nuclear potential $V_N(r=R_{cr})$ available

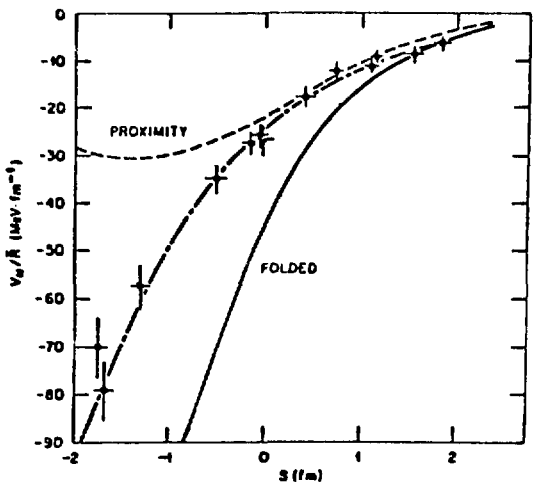

Fig. 12 Nuclear potentials at the critical radius R_{cr} deduced from fusion cross sections. The proximity potential[13] is plotted for b = 1 fm.

from high-energy data, plotted vs. the separation of the nuclear surfaces $s=r-R_1-R_2$, where R_1,R_2 are taken to be the radii of the half-central-density points of the nuclei. On this scale, the strong absorption radius (5) occurs at $s \approx 2.5$ fm. Also, as suggested by eq. (6), V_N is scaled by their mean radius of curvature $\bar{R} = R_1R_2/(R_1+R_2)$ to provide a 'universal' curve. This approach provides values of V_N as deep as 100-115 MeV (for $^{20}Ne + {}^{24}Mg$, ^{27}Al: see ref. 44), and values of R_{cr} ($s \approx -2$ fm) corresponding to appreciable overlap of the nuclear surfaces. The values of R_{cr} were deduced assuming the moment of inertia to be that of separated spheres, $J = \mu R_{cr}^2$. Some 'sticking' of the two nuclei would result in larger values of J, and the values of R_{cr} then deduced would be somewhat smaller[8,42].

Also shown in fig. 12 are the predictions of a double-folding model which accounts successfully[15] for scattering data that are sensitive to the potential at larger s-values, as well as the proximity potential[13]. The 'measured' values fall between. However, we emphasize again that the validity of the simple potential model, and the precise significance of the potential, has not yet been determined[2].

The possible effects on the fusion process of the nucleus-nucleus potential being non-spherical (because one or both nuclei are deformed) has also received attention recently[45]. Then the potential barrier may depend sensitively upon the relative orientation of the two nuclei and, particularly at low energies, may result in penetrabilities very different from the assumption of a spherical potential.

3.5 SPIN-DEPENDENCE

Earlier, it was common to think that spin-orbit coupling for heavy ions arose only from the odd, valence nucleon(s), thus it was a "1/A" effect and much weaker than for light ions. Explicit folding model calculations[46] appeared to support this conclusion. However, experimental evidence has been accumulating that this is completely wrong. Spin-dependent effects are much stronger, and their observation provides a rich new field for the study of heavy-ion interactions. Current theoretical analyses are ascribing the spin-dependence to the coupling to various non-elastic channels. This raises the interesting question whether such studies can suggest certain universal features of the effective spin coupling, or whether each case has to be treated individually because it depends in detail on the specific channels available.

The experimental evidence is both direct and indirect. The former consists of measuring the vector analyzing powers for the elastic scattering of polarized beams, and is confined to ^{6}Li and ^{7}Li ions at quite low energies[47,48]. Nonetheless, the spin-orbit coupling required to explain these data is very much stronger than folding models[46] predict; indeed for ^{7}Li, it has the opposite sign. Indirect evidence comes from non-elastic reactions which appear to require the introduction of strong spin couplings for their explanation[48,49].

The theoretical explanation offered[50] is that the spin coupling is an effective one, arising from couplings to inelastic and/or transfer channels (i.e. it is contained in the ΔU of eqs. (2) and (3)). Thus the precise nature (including sign) of the effective coupling for any particular projectile-target system depends upon the spins of the strongly coupled intermediate states and the angular momentum transfers involved in their excitation. When the target spin is negligible, and the projectile has spin I, the effective coupling can always be written as proportional to the usual vector spin-orbit $\underset{\sim}{L}\cdot\underset{\sim}{I}$ (plus tensors of higher rank if $I > 1/2$), but the coefficients will be non-local and depend upon the magnitude of L. Some local approximation has to be found before it can be compared to phenomenological spin-orbit potentials. Explicit calculations[50] indicate that such an effective coupling can be one or two orders of magnitude stronger than that obtained from a simple folding model[46].

4. Some potential models

4.1 INTERACTION ENERGY FUNCTIONS

The uncertainties over how to use many calculated (and real) 'potentials' (= interaction energies) were discussed in Sec. 2. Such potentials tend to be similar for separated nuclei ($r \sim R_{SA}$ or $s \gtrsim 2$ fm), where their behavior is characterized by eq. (6) and where there is most justification for simply using them in the Schrödinger equation (4). Thus they might be appropriate for describing 'low' energy scattering which does not sense smaller separations. However, the interaction energy is quite weak in this region (~ 1 MeV) and behaving exponentially, so that it is quite sensitive to the physics input. Thus, close agreement with scattering data might not be expected unless the calculation was designed with that in mind. One such calculation using that constraint was based upon the microscopic-macroscopic approach[14] and yielded reasonable agreement with some elastic data. This potential is not defined for $s < 0$. Another popular potential is based upon the proximity theorem and the Thomas-Fermi model[13]. Elastic scattering was not used to constrain the parameters of the calculation and the predicted potential usually requires some adjustment in order to fit measured scattering. The superposition of two 'frozen' densities is assumed and the proximity energy includes contributions from changes in the kinetic energies of the nucleons. Consequently the 'potential' becomes less attractive (minimum at $s \approx -1.3$ fm), and finally repulsive ($s \lesssim -3$ fm), as the nuclei overlap (see fig. 12).

4.2 FOLDING MODEL

Another potential model is derived from the double-folding expression

$$U_F(\underset{\sim}{r}) = \iint \rho_1(\underset{\sim}{r}_1)\rho_2(\underset{\sim}{r}_2)v(\underset{\sim}{r}+\underset{\sim}{r}_2-\underset{\sim}{r}_1)d\underset{\sim}{r}_1 d\underset{\sim}{r}_2, \tag{11}$$

where $\rho_i(\underset{\sim}{r}_i)$ is the density distribution for nucleus i and v is some effective nucleon-nucleon interaction. A popular model for v (the M3Y) is based upon the (real) G-matrix for two nucleons bound in a nucleus[51] and includes an approximate correction for the exchange of the two interacting nucleons. The model (11) is supposed to represent the first term U_F of the Feshbach potential (2), (3); thus it is appropriate to use it as an optical potential. It is implicitly assumed that the remainder ΔU is predominantly imaginary and is to be represented by a phenomenological absorptive potential. One advantage of this model is that one may incorporate structure information, such as shell effects, in the nuclear densities. In contrast to the proximity potential, eq. (11) gives very deep potentials at small distances (fig. 12). The model has been extensively reviewed elsewhere[1,15]. Suffice it to say that, with the M3Y interaction[51], it has had considerable success in interpreting elastic data which are dominated by peripheral collisions[15,52]. Somewhat surprisingly, it also seems to be compatible with some cases which are sensitive to the potential at smaller radii[24,37], such as the $^{12}C+^{12}C$ system at 300 MeV mentioned in Sec. 3.3 (figs. 6 and 7). Exceptions occur for the weakly-bound projectiles $^{6,7}Li$ and ^{9}Be, but the failure of the M3Y interaction for these appears to be understood now in terms of break-up effects[53].

The M3Y model for v does not depend upon the density or the energy. Density dependence is required for a detailed understanding of nucleon-nucleus potentials, and had to be introduced in order to fit alpha scattering in the 'rainbow' region[54]. However, no significant density dependence appears to be allowed by the 300-MeV $^{12}C+^{12}C$ results. On the other hand, there is clear evidence from $^{12}C + ^{12}C$ at 1016 MeV that the potential must decrease in strength as E increases. Finally, any theory of the effective interaction which recognizes the presence of open channels will yield a complex v. More recent studies[55] derive a G-matrix for two interacting nucleons embedded within two pieces of nuclear matter that are flowing through each other. This effective interaction is complex and depends upon energy and density. It is used in eq. (11) by evaluating it at the local density $\rho_1 + \rho_2$ midway between the two nucleons. However, uniform nuclear matter neglects surface effects, such as collective shape oscillations and transfer processes, so that the potential (11) has to be supplemented by surface contributions calculated (in a semi-phenomenological way) according to eq. (3) for ΔU. In the one system so far studied[55], $^{16}O + ^{16}O$, both the real and imaginary parts of ΔU dominated over U_F in the important surface region. This violates the assumption made in applications of the simple M3Y folding model that $\mathrm{Re}\Delta U$ is negligible. Clearly, further applications of this approach are needed; $^{12}C + ^{12}C$ at 300 MeV would be an interesting example.

4.3 SURFACE INTERACTIONS

Other calculations, like that just mentioned, have been made for ΔU, taking account of surface excitations[40]. When the bombarding energy is much greater than the excitation energy, the process is sudden and the contribution to ΔU is predominantly imaginary[40,56,57]. When the two energies are comparable, the process is more adiabatic, the system readjusts and ΔU tends to be real[58]. The long-ranged polarization potentials that arise from Coulomb excitation[40,56,58] provide one example of each.

An illuminating study[59] of the sources of peripheral absorption was made using a semi-classical approximation. It made clear that single-nucleon transfer reactions should give rise to an absorptive potential that has a longer range in the surface (exponential decay length ~ 0.5 fm) than does the absorption due to collective surface excitations (~ 0.3 fm). Which process dominates depends upon the available excited states, as well as the bombarding energy; there is some

indication that transfer is the most important source of absorption at large radii ($r \geq R_{SA}$). It is interesting that the transfer contributions to $\mathrm{Im}\Delta U$ for ^{16}O + ^{28}Si show the same tendency to decrease with decreasing energy that is found empirically (fig. 11).

5. Acknowledgment

The research was sponsored by the Division of Nuclear Physics, U.S. Department of Energy, under Contract W-7405-eng-26 with the Union Carbide Corporation.

6. References

1) G.R. Satchler, Direct nuclear reactions (Oxford University Press, 1983), and other references cited there
2) H.J. Krappe, Proc. symp. on deep-inelastic and fusion reactions with heavy ions (Berlin, 1979); Lecture notes in physics 117 (1980) 212
3) H. Feshbach, Ann. Phys. (New York) 19 (1967) 287
4) K. Wildermuth and Y.C. Tang, A unified theory of the nucleus (Academic Press, 1977); M.V. Mihailovic and M. Rosina, Generator-coordinate method for nuclear bound states and reactions, Fizika Suppl. 5 (1973); Y.C. Tang, M. LeMere and D.R. Thompson, Physics Reports 47 (1978) 167
5) H. Friedrich, Physics Reports 74 (1981) 209
6) S. Okabe, to be published; H. Horiuchi, to be published
7) D. Pal, J.R. Rook and A.M. Kobos, Nucl. Phys. A348 (1980) 45
8) U. Mosel Particles & Nuclei 3 (1972) 297
9) W.E. Frahn, in Heavy-ion science, Vol. 1 (ed. D.A. Bromley, Plenum Press, 1982)
10) W.U. Schroeder and J.R. Huizenga, Ann. Revs. Nucl. Sci. 27 (1977) 465
11) M.H. Macfarlane and S.C. Pieper, Phys. Lett. 103B (1981) 169
12) P.R. Christensen and A. Winther, Phys. Lett. 65B (1977) 19; R.O. Akyuz and A. Winther, in Proc. int. school of physics 'Enrico Fermi', 1979 (eds. R.A. Broglia, C.H. Dasso and R. Ricci, North-Holland, 1980); M. Lozano and G. Madurga, Nucl. Phys. A334 (1980) 349
13) J. Blocki, J. Randrup, W.J. Swiatecki and C.F. Tsang, Ann. Phys. (New York) 105 (1977) 427
14) H.J. Krappe, J.R. Nix and A.J. Sierk, Phys. Rev. C 20 (1979) 992
15) G.R. Satchler and W.G. Love, Physics Reports 55 (1979) 183
16) R.A. Broglia and A. Winther, Heavy-ion reactions (Benjamin/Cummings, 1981)
17) W.G. Lynch, M.B. Tsang, H.C. Bhang, J.G. Cramer and R.J. Puigh, Phys. Rev. Lett. 48 (1982) 979
18) D.M. Brink, in Les Houches, Session XXX, Nuclear physics with heavy ions and mesons (North-Holland, 1978); C. Marty, Lecture notes on analysis of heavy-ion scattering amplitudes (Orsay internal report IPNO/TH 79-3, 1978); K.W. McVoy, Semiclassical methods and surface creep waves in heavy-ion reactions, Notas de fisica 1, No. 4 (Universidad Nacional Autonoma de Mexico, 1978)
19) N. Rowley and C. Marty, Nucl. Phys. A266 (1977) 494
20) R.M. DeVries et al., Phys. Rev. Lett. 39 (1977) 450
21) P. Schwandt et al., Phys. Rev. C 21 (1980) 1656
22) J.G. Cramer and R.M. DeVries, Phys. Rev. C 22 (1980) 91
23) H.G. Bohlen et al., Zeit Phys. A308 (1982) 121
24) M.E. Brandan, Phys. Rev. Lett. 49 (1982) 1132
25) M. Buernerd et al., Phys. Rev. C 26 (1982) 1299
26) J. Cook et al., to be published
27) D.A. Goldberg, S.M. Smith and G.F. Burdzik, Phys. Rev. C 10 (1974) 1362
28) K.W. McVoy et al., to be published
29) D.M. Brink and N. Takigawa, Nucl. Phys. A279 (1977) 159

30) J. Albinski and F. Michel, Phys. Rev. C 25 (1982) 213
31) E. Friedman, H.J. Gils, H. Rebel and R. Pesl, Nucl. Phys. A363 (1981) 137, and other references given there
32) R.S. Mackintosh and A.M. Kobos, Phys. Lett. 92B (1980) 59
33) J. Barrette and S. Kahana, Comm. Nucl. Part. Phys. 9 (1980) 67
34) A.M. Kobos and R.S. Mackintosh, to be published
35) S. Krewald, A. Djaloeis and S. Gopal, Phys. Rev. C 24 (1981) 966
36) A.M. Kobos and R.S. Mackintosh, Phys. Rev. C 26 (1982) 1766
37) A.M. Kobos, G.R. Satchler and R.S. Mackintosh, Nucl. Phys. A395 (1983) 248
38) S. Kahana et al., to be published
39) M.F. Vineyard, J. Cook and K.W. Kemper, to be published
40) M.A. Franey and P.J. Ellis, Phys. Rev. C 23 (1981) 787; A.J. Baltz et al., Nucl. Phys. A327 (1979) 221
41) L.C. Vaz et al., Physics Reports 69 (1981) 373
42) D. Glas and U. Mosel, Nucl. Phys. A237 (1975) 429
43) J. Gomez del Campo et al., to be published
44) Nguyen Van Sen et al., Phys. Rev. C 27 (1983) 194; M. Albinska et al., Phys. Rev. C 27 (1983) 207
45) R.G. Stokstad and E.E. Gross, Phys. Rev. C 23 (1981) 281; M.J. Rhoades-Brown et al., Zeit. Phys. A310 (1983) in press; M.J. Rhoades-Brown and V.E. Oberacker, to be published
46) F. Petrovich et al., Phys. Rev. C 17 (1978) 1642; P.J. Moffa, Phys. Rev. C 16 (1977) 1431; H. Amakawa and K.I. Kubo, Nucl. Phys. A266 (1976) 521
47) D. Fick, Ann. Revs. Nucl. Part. Sci. 31 (1981) 53, and other references given there
48) Polarization phenomena in nuclear physics, AIP Conf. Proc. 69 (1981) 1000
49) S. Kubano et al., Phys. Rev. Lett. 38 (1977) 817; P. Wust et al., Zeit Phys. A291 (1979) 151; W. Dunnweber et al., Phys. Rev. Lett. 43 (1979) 1642; W. von Oertzen et al., Zeit. Phys. A301 (1981) 365, and to be published; M. Tanaka et al., Phys. Lett. 106B (1981) 293
50) H. Nishioka et al., Phys. Rev. Lett. 48 (1982) 1795; H. Ohnishi et al., Phys. Lett. 118B (1982) 16; B. Imanishi and W. von Oertzen, Phys. Lett. 118B (1982) 273; S. Chakravati et al., Phys. Rev. C 27 (1983) 143; Q.K.K. Liu submitted to this meeting
51) G. Bertsch et al., Nucl. Phys. A284 (1977) 399
52) G.R. Satchler, Nucl. Phys. A329 (1979) 233
53) I.J. Thompson and M.A. Nagarajan, Phys. Lett. 106B (1981) 161; R.S. Mackintosh and A.M. Kobos, Phys. Lett. 116B (1982) 95
54) A.M. Kobos et al., Nucl. Phys. A384 (1982) 65
55) S.B. Khadkikar et al., Nucl. Phys. A369 (1981) 495, and other references there
56) N. Vinh Mau, Phys. Lett. 71B (1977) 5
57) W.G. Love et al., Nucl. Phys. A291 (1977) 183
58) J. Rasmussen et al., Nucl. Phys. A341 (1980) 149
59) R.A. Broglia et al., Nucl. Phys. A361 (1981) 307; G. Pollarolo et al., Nucl. Phys., to be published

DISCLAIMER

This report was prepared as an account of work sponsored by an agency of the United States Government. Neither the United States Government nor any agency thereof, nor any of their employees, makes any warranty, express or implied, or assumes any legal liability or responsibility for the accuracy, completeness, or usefulness of any information, apparatus, product, or process disclosed, or represents that its use would not infringe privately owned rights. Reference herein to any specific commercial product, process, or service by trade name, trademark, manufacturer, or otherwise does not necessarily constitute or imply its endorsement, recommendation, or favoring by the United States Government or any agency thereof. The views and opinions of authors expressed herein do not necessarily state or reflect those of the United States Government or any agency thereof.